# Journal Pre-proofs

Deep Learning-Enabled Hyperspectral Classification of Zhambons

Seyedehsamaneh Shojaeilangari, Esmat Kishani Farahani, Alireza Bassiri

Please cite this article as: Seyedehsamaneh Shojaeilangari, Esmat Kishani Farahani, Alireza Bassiri, Deep Learning-Enabled Hyperspectral Classification of Zhambons, *Innovative Food Technologies (2025)*, doi: https://doi.org/ 10.22104/ift.2025.8010.2255

This is a PDF file of an article that has undergone enhancements after acceptance, such as the addition of a cover page and metadata, and formatting for readability, but it is not yet the definitive version of record. This version will undergo additional copyediting, typesetting and review before it is published in its final form, but we are providing this version to give early visibility of the article. Please note that, during the production process, errors may be discovered which could affect the content, and all legal disclaimers that apply to the journal pertain.

# Deep Learning-Enabled Hyperspectral Classification of Zhambons

**Seyedehsamaneh Shojaeilangari[1,*], Esmat Kishani Farahani [2], Alireza Bassiri[3]**

*1 Biomedical Engineering Group, Department of Electrical Engineering and Information Technology, Iranian Research Organization for Science and Technology (IROST), 33535111, Tehran, Iran*

*2 Information Technology and Intelligent Systems Group, Department of Electrical Engineering and Information Technology, Iranian Research Organization for Science and Technology (IROST), 33535111, Tehran, Iran*

*3 Department of Chemical Technologies, Iranian Research Organization for Science and Technology (IROST), 33535111, Tehran, Iran*

*[*] Corresponding author: Seyedehsamaneh Shojaeilangari (E-mail: s.shojaie@irost.ir)*

## Abstract

Food authenticity is a crucial aspect of consumer protection, food safety, and quality assurance. Conventional methods for meat authentication often require destructive, time-consuming, or labor-intensive processes. Hyperspectral imaging, which combines imaging and spectroscopy, has emerged as a non-destructive alternative for food classification. This study investigates the application of hyperspectral imaging for differentiating between beef, chicken, and turkey zhambons using one-dimensional convolutional neural networks and long short-term memory networks. Following preprocessing—including segmentation, noise reduction, and spatial averaging—spectral signatures were extracted and classified using deep learning models and then compared to traditional machine learning approaches. The long short-term memory architecture demonstrated superior performance by effectively modeling sequential spectral dependencies, achieving 99.94% accuracy in the binary classification of chicken versus beef and 98.12% accuracy in the three-class problem (beef, chicken, and turkey zhambons). The findings highlight the potential of hyperspectral imaging combined with machine learning approaches as an efficient tool for processed meat authentication.

## Keywords

Convolutional neural network, deep learning, hyperspectral imaging, long short-term memory, machine learning, processed meat authentication.

## 1. Introduction

Food fraud, particularly concerning meat authenticity, poses a substantial threat to food safety, consumer confidence, and economic stability [1], [2], [3], [4], [5]. This issue extends beyond simple adulteration—where inferior substances are intentionally mixed in—to the critical verification of a product's true origin and composition. For instance, in processed meats like zhambons, ensuring they are made from declared species such as beef, chicken, or turkey without unauthorized substitution is paramount. Such deceptions result in direct economic losses for consumers and producers, while also introducing health hazards and ethical dilemmas, especially in products where post-processing creates a uniform texture and appearance that evades visual inspection. Traditional methods for species identification, such as PCR-based molecular techniques and chemical analyses, provide high accuracy but are inherently destructive, time-consuming, and impractical for real-time industrial applications [6], [7], [8]. These limitations underscore the urgent need for innovative, non-invasive technologies to safeguard the integrity of the global meat supply chain.

Hyperspectral imaging (HSI) represents a promising non-destructive alternative, seamlessly integrating spectroscopy with digital imaging to acquire both spatial and spectral data across

wavelength ranges of 400-2500 nm. This technology enables precise chemical profiling of meat, capturing signatures related to composition, freshness, and origin without altering the sample. When paired with deep learning (DL) models, which excel at autonomously extracting intricate features from complex HSI datasets, HSI becomes a powerful tool for automated food authentication, fraud detection, and traceability. [9], [10], [11], [12], [13]. The synergy of HSI and DL not only enhances detection speed and accuracy but also addresses key barriers in food safety applications, such as the scarcity of labeled training data and the demand for interpretable models to meet regulatory standards [14], [3].

The literature indicates significant advancements in predicting food spoilage through ML, with recent work by Ince et al. combining explainable artificial intelligence (AI) and data augmentation for more accurate sausage spoilage intensity prediction [15]. This approach addresses critical challenges including limited labeled data availability and the need for model transparency, particularly important in food safety applications where understanding prediction rationale is essential for regulatory compliance. Research has evolved from traditional microbiology approaches focused on specific spoilage organisms like Lactobacillus sakei and Leuconostoc gelidum to sophisticated AI-driven methods that enable non-destructive, rapid assessment of spoilage levels, potentially reducing food waste while maintaining consumer protection.

Yu et al. used hyperspectral imaging for distinguishing fresh, frozen, and multi times frozen and thawed beef cuts. They used support vector machine (SVM), partial least squares discriminant analysis (PLS-DA), and artificial neural network (ANN) while achieved the best results of 97.83% for SVM [16]. A key innovation was their method of separately analyzing fat and muscle tissues, which performed significantly better than models based on overall beef cut averaging. The researchers also created visualization maps showing the spatial distribution of deterioration indices across beef samples. Their findings demonstrated that repeated freeze-thaw cycles cause detectable changes in the spectral characteristics of beef, particularly around bands associated with respiratory pigments (550, 572, and 650 nm), reflecting oxidation of hemoglobin and myoglobin as well as moisture loss during freezing and thawing processes. They developed a portable HSI and investigated beef adulteration with institution of parts of chicken and duck. They achieved the accuracy of 94.91% by applying a model based on SVM with spectral space transformation (SST) [2].

Siddique et al. developed innovative predictive classification models using near-infrared (NIR) spectroscopy to identify spoilage in chicken breast fillets [17]. Their research utilized a portable hyperspectral device operating across 350-2500 nm wavelengths to analyze chicken samples stored at 4°C, while conducting aerobic plate counts to establish microbial spoilage thresholds. They classified spoilage into three stages: initiation (≤3 log CFU/ml), propagation (3-6.9 log CFU/ml), and spoiled (>7 log CFU/ml). Employing ANNs and linear SVMs with ten-fold cross-validation, they achieved classification accuracies of 93.7%, 95.2%, and 98% for the respective spoilage stages. The study identified signature wavelengths that effectively indicated chicken spoilage, offering potential for developing cost-effective detection systems that could help minimize food waste through rapid, non-destructive spoilage detection.

In a similar study, Zheng et al. demonstrated the efficacy of visible near-infrared (Vis-NIR) hyperspectral imaging for detecting duck meat adulteration in minced lamb meat as a non-destructive and rapid analytical method [18]. The researchers developed a system operating across the 400-1000 nm spectral range to analyze minced lamb samples adulterated with varying percentages of duck meat. Using multivariate analysis techniques coupled with ML algorithms,

they achieved impressive classification accuracies exceeding 95% for identifying adulteration levels. The study highlighted several key wavelengths that served as effective markers for detecting duck meat contamination.

Kamruzzaman et al. presented a rapid and efficient method for detecting and visualizing adulteration in minced lamb meat using NIR hyperspectral imaging and multivariate image analysis [19]. The researchers employed a hyperspectral imaging system to analyze minced lamb meat samples adulterated with varying levels of other meat types. Using advanced multivariate data analysis techniques and classification algorithms, they achieved high accuracy (exceeding 90%) in detecting adulteration percentages and providing visual representation of the results. This research not only offered a non-destructive and rapid detection method but also enabled spatial visualization of the distribution of different components within the sample.

In another study, Cruz-Tirado et al. investigated the detection of adulteration in alpaca meat using a combination of portable NIR spectrometry and NIR-HSI coupled with advanced chemometric methods [20]. Alpaca meat, valued for its high protein content, good tenderness, and low intramuscular fat, commands premium prices compared to conventional meats, making it susceptible to economic adulteration. The researchers evaluated both technologies for detecting adulterations with pork, chicken, and beef in concentrations ranging from 0-50% (w/w). Their spectral analysis revealed significant differences in the spectra of pure meat samples using NIR-HSI, primarily associated with fatty acid composition variations between meat types. The study implemented principal component analysis (PCA) to group samples into pure and adulterated alpaca meat classes, followed by the development of data driven soft independent class analogy (DD-SIMCA) models that achieved notable authentication results with above 99.7% sensitivity and specificity. For quantification of adulterants, the researchers employed partial least squares regression (PLSR) models, with NIR-HSI outperforming the portable NIR spectrometer, yielding residual predictive deviation (RPD) values of 3.39-10.19 and root mean square error of prediction (RMSEP) values of 1.53-3.93%. These findings demonstrate that both technologies, particularly when supported by appropriate chemometric methods, can be effectively implemented as rapid screening tools to detect fraud in premium alpaca meat products.

All these researches represent a significant advancement in food authentication technology, offering potential for integration into processing lines for real-time monitoring of meat product integrity and addressing growing consumer concerns about food fraud in the meat industry [19], [21], [22], [23], [24], [25], [26], [27], [28], [29]. However, most prior research has focused on raw or minimally processed meat, leaving processed products such as zhambons—which undergo curing, cooking, and blending—largely unexplored. These processing steps alter spectral characteristics, increase overlap between meat types, and pose significant challenges for accurate authentication using conventional methods.

Moreover, economic incentives drive fraudulent practices, such as substituting chicken for beef, highlighting the critical need for reliable, non-destructive, and rapid authentication methods to protect consumers and maintain food quality standards. While traditional machine learning approaches have shown promise, they often rely on extensive feature engineering and fail to fully exploit the sequential dependencies inherent in hyperspectral signatures, limiting their generalization performance in real-world scenarios.

Building on these advancements and addressing the remaining challenges, this study applies DL– enhanced hyperspectral imaging to authenticate zhambons from beef, chicken, and turkey. We develop and evaluate both one-dimensional convolutional neural networks (1D-CNN) and long short-term memory (LSTM) networks, with the LSTM explicitly designed to capture sequential

spectral dependencies. The 1D-CNN serves as a comparative DL baseline, while both models are compared to conventional machine learning algorithms to assess robustness, classification accuracy, and computational efficiency under limited labeled data conditions.

Accordingly, this study is designed with the following objectives:

1. To acquire hyperspectral imaging data from beef, chicken, and turkey zhambon samples under controlled conditions.
2. To extract and preprocess spectral signatures to enhance data quality and minimize noise.
3. To develop, train, and evaluate 1D-CNN and LSTM models for the classification of meat types.
4. To compare the performance of these DL models with conventional machine learning algorithms in terms of accuracy, robustness, and computational efficiency.

Through this research, we aim to advance the application of DL–driven hyperspectral imaging as a reliable, scalable, and non-destructive solution for processed meat authentication, addressing a critical need for transparency, fraud prevention, and quality assurance in the global food supply chain. The analyses provide a comprehensive evaluation of both predictive capability and practical feasibility, supporting the potential integration of hyperspectral imaging with advanced modeling techniques in real-world meat quality control.

The remainder of this paper is organized as follows: Section 2 presents materials and methods including materials, sample preparation, hyperspectral image acquisition, spectral preprocessing, deep and classical architectures, and experimental setup. Results and discussion are presented in Section 3. Section 4 concludes the paper.

## 2. Materials and Methods

Figure 1 provides a comprehensive overview of the study workflow. The primary objective of this study is to develop a robust DL framework for the classification of zhambon samples from different species (beef, chicken, and turkey) using HSI. Hyperspectral data were acquired across the 400–950 nm range, capturing both spatial and spectral information relevant to meat composition. Spectral preprocessing was applied to reduce noise and enhance meaningful features, providing reliable inputs for model training. DL models were developed and systematically evaluated for their ability to accurately classify the species of each sample. To ensure robust model assessment, we employed a Leave-One-Slice-Out (LOSO) cross-validation strategy. In each fold, a single slice per species served as the test set, with the remaining four slices forming the training pool. Within this pool, one slice was allocated as a validation set for hyperparameter optimization, while the other three were used for initial training. After tuning, the model was retrained on all four training/validation slices and then evaluated on the independent test slice, ensuring a rigorous measure of generalizability while accounting for data-splitting variability. In addition, the performance of the DL models was compared with conventional ML algorithms in terms of classification accuracy, robustness, and computational efficiency.

### 2.1 Materials

Samples were prepared using meat from three different animal species: beef, chicken and turkey, which were sourced from local butchers in Tehran.

### 2.2 Sample Preparation

Samples were prepared, using the method described by Vercammen et al. [30]. The final concentrations of used ingredients in the finished products were 18 g/kg salt, 0.120 g/kg sodium nitrite, 0.5 g/kg sodium ascorbate, 5 g/kg glucose, 3 g/kg phosphate.

All samples followed consistent curing and processing procedures to ensure uniformity across all samples. Each formulation contained identical proportions of meat, curing salt, and other ingredients to minimize variability due to composition. This standardized preparation ensured that any observed spectral differences could be attributed primarily to the intrinsic characteristics of the meat species rather than to processing or formulation discrepancies.

After production, all samples were vacuum-sealed and stored under refrigeration at $5 \pm 1$ °C for one day to preserve freshness and prevent microbial growth. Prior to imaging, the samples were brought to room temperature (approximately $24 \pm 1$ °C) for about 30 minutes to equilibrate surface moisture and temperature, which are known to influence spectral reflectance measurements.

For imaging, each type of zhambon was sectioned into uniform slices using a clean steel knife to prevent cross-contamination. Five representative slices were prepared from each meat type, with precise dimensions of 10.5 mm × 10.5 mm × 4 mm (length × width × thickness), as illustrated in Figure 2. All slices were placed on a non-reflective black background to minimize scattering effects and ensure consistent illumination during hyperspectral data acquisition.

The sample preparation protocol was designed to provide uniform sample geometry and surface characteristics, which are critical for obtaining high-quality hyperspectral images and reliable spectral data for subsequent DL analysis.

## 2.3 Hyperspectral Imaging Acquisition

A line-scanning hyperspectral imaging system (a desktop model produced by Parto Afzar Sannat Company, Zanjan, Iran [31]) was used for image acquisition. The system consisted of three halogen lamps, a hyperspectral camera, and a scanner controlled by a PC. The camera covers the visible to near-infrared range of 400–950 nm with 993 spectral bands (approximately 0.55 nm spectral resolution). The spatial resolution of the camera is 210 μm. The maximum scan length of the system is 20 cm.

First, the system's light source was turned on. After 2.5 minutes, when the light spectra became stable, the system was calibrated using a white reference paper and the black cap of the camera lens. Scan length was set on 110 mm. Hyperspectral images were captured from both the top and bottom sides of each slice (Figure 3). Totally 30 images were captured, consisting of 5 slices per zhambon, 2 sides per slice, and 3 types of zhambons. Therefore, 10 images were captured for each zhambon type.

## 2.4 Spectral Preprocessing

Prior to data analysis, each acquired image underwent a systematic preprocessing and segmentation pipeline to isolate regions of interest and standardize input data.

**Segmentation:** The process commenced with the reading of the raw image file into a digital matrix representing pixel intensities. A specific region of interest (ROI) was then manually defined to exclude extraneous background and focus the analysis solely on the relevant meat sample, thereby reducing computational noise. This ROI was subsequently partitioned into non-overlapping cubes of 10 × 10 × 990 pixels, after removing the first and last few wavelength bands that typically exhibit low signal quality in the captured data. This grid-based segmentation approach serves an important purpose: it enables localized analysis by dividing the heterogeneous sample into smaller regions. From each slice, approximately 120 spectral blocks were extracted. With 5 slices per zhambon and 2 sides per slice, this process produced a total of ~1,200 blocks per meat category (beef, chicken, or turkey). Each resulting 10 × 10 pixel cube was subsequently treated as an individual data unit for further analysis.

- **Noise reduction:** Raw hyperspectral image cubes were preprocessed using a Savitzky-Golay filter [32] to mitigate high-frequency noise. The Savitzky-Golay filter's ability to effectively reduce noise while preserving the shape and features of spectral signatures makes it an ideal choice for hyperspectral data processing across a wide range of applications in remote sensing, agriculture, environmental monitoring, and other fields [32], [33], [34], [35]. A polynomial order of 3 and a window size of 7 spectral channels were selected to effectively smooth the data while preserving the integrity of critical absorption features essential for accurate classification. This window length was chosen to correspond with the instrument's spectral resolution, achieving optimal noise reduction without causing significant feature distortion.
- **Averaging:** After applying the Savitzky-Golay filter, the hyperspectral cube was spatially averaged within each block to generate a representative mean spectrum. For each $10 \times 10$ pixel block, the mean reflectance was computed across all 990 spectral bands, producing a one-dimensional vector of size $1 \times 990$. This approach preserves the localized spectral information while reducing noise, resulting in multiple spectra per sample (~120 per slice). Each vector captures the dominant spectral characteristics of its corresponding block and serves as input for subsequent discriminative analysis.

## 2.5 Deep Architectures

While DL–based classification offers significant advantages for hyperspectral data analysis, the practical implementation of such models requires careful architectural design. In particular, the high dimensionality of hyperspectral data can lead to models with a large number of parameters, which increases the risk of overfitting when training data are limited. To address this issue, the architectures proposed in this study are intentionally designed to be shallow, balancing model complexity, computational efficiency, and generalization capability. This design choice reflects an implementation-level consideration specific to the developed models. The following section details the network architectures and explains how these design principles are realized in practice.

### 2.5.1 1D-CNN

As a first DL model, a 1D-CNN, as shown in Figure 4, is designed to process raw spectral signals without normalization, preserving the absolute intensity values critical for classification. The network begins with three convolutional blocks that progressively extract features at various scales using decreasing kernel sizes (11, 7, 5) and an increasing number of filters (32, 64, 128). Each block incorporates batch normalization and ReLU activation for stable and efficient training, followed by max-pooling layers in the first two blocks to reduce dimensionality and emphasize dominant features. The final convolutional features are aggregated into a compact representation via global average pooling, which is then fed into a series of fully connected layers with dropout regularization to mitigate overfitting before the final softmax classification layer. This design allows the model to hierarchically learn discriminative patterns directly from the raw spectral data, from local spectral shapes in the early layers to broader, more abstract features in the deeper layers.

### 2.5.2 LSTM

The second DL architecture, illustrated in Figure 5, incorporates an LSTM network designed to hierarchically extract and model temporal dependencies within the spectral data. The model begins by processing the input sequence through an LSTM layer with 32 units, configured to return the full sequence of hidden states to preserve temporal information for subsequent layers. This is followed by batch normalization, a ReLU activation function, and a dropout layer for

regularization. This vector is subsequently fed through a series of fully connected layers with non-linear activations and additional dropout to further refine the feature representation before the final softmax classification layer. This hierarchical structure allows the network to learn complex, multi-scale patterns inherent in the data, making it well-suited for the sequence classification task.

## 2.6 Classical Architectures

In addition to our designed DL models (1D-CNN and LSTM), classical ML classifiers including SVM [36], random forest (RF) [37], and gradient boosting (GB) [38] are investigated. 11 hand-crafted statistical features including mean, standard deviation, maximum, minimum, range, skewness, kurtosis, median, interquartile range (IQR), median absolute deviation, and spectral area are used as input features. These features are selected because they represent both the central tendency and higher-order variability of spectral signatures.

SVM works by finding an optimal hyperplane that maximizes the margin between different classes in the feature space. It was used by RBF kernel. The RBF kernel transforms the original feature space into a higher-dimensional space, enabling the modeling of non-linear relationships.

RF operates by constructing multiple decision trees during training and outputting the class that is the mode of the classes from individual trees. This ensemble approach reduces overfitting and improves generalization by aggregating predictions from diverse trees.

GB builds models sequentially, with each new model correcting errors made by the previous ones. This adaptive approach enables GB to focus learning on difficult-to-classify samples, gradually improving performance on challenging cases. Grid search technique was applied to optimize the parameters of each classifier.

## 2.7 Experimental Setup

The experiments were conducted using MATLAB 2022 alongside Python 3.12, executed on a desktop workstation equipped with an NVIDIA GeForce RTX 4060 Ti GPU featuring 16 GB of memory. The training process and evaluation methodology were meticulously designed to facilitate robust model development and to provide a comprehensive performance assessment, as detailed in the following sections.

**Dataset Partitioning:** To facilitate a rigorous evaluation and mitigate overfitting, we implemented a Leave-One-Slice-Out (LOSO) cross-validation strategy. In each fold, one slice per species was held out as the test set, while the remaining four slices constituted the training pool. From these four, one slice was reserved as a validation set for hyperparameter tuning, with the other three used for initial model training. After determining the optimal hyperparameters on the validation slice, the model was retrained using all four training and validation slices and then evaluated on the held-out test slice. This process was repeated such that each slice served once as an independent test set, thereby eliminating any cross-slice information leakage. To ensure statistical reliability, reproducibility, and model stability, all results are reported as the average performance metrics along with their standard deviation.

**Optimization Algorithm:** The model was optimized using the adaptive moment estimation (Adam) optimizer [39]. Adam was selected for its efficiency and effectiveness in handling sparse gradients on noisy problems, which is common in DL tasks.

**Loss Function:** Given the multi-class classification nature of the task, the model was trained by minimizing the categorical cross-entropy loss function [40]. This loss function measures the dissimilarity between the true class distribution (ground truth labels) and the predicted probability distribution generated by the model's softmax output layer, providing a strong gradient for correct class probability maximization.

**Evaluation Metrics:** Model performance was evaluated using a suite of standard classification metrics to provide a holistic view of its capabilities. The primary metrics reported are accuracy, precision, recall, and F1-score.

## 3. Results and Discussion

This section presents an extensive evaluation of the designed neural network architectures, specifically the 1D-CNN and LSTM models, developed for hyperspectral meat classification tasks. We systematically assessed these models across two classification scenarios: a binary classification distinguishing between beef and chicken zhambon products, and a more challenging multi-class classification differentiating between beef, chicken, and turkey zhambon varieties. Prior to implementing these DL approaches, we conducted a preliminary visual examination of the spectral signatures from our three meat categories to identify potential distinguishing characteristics in their reflectance patterns.

### 3.1 Spectral Characteristics

The visual inspection of spectral data served as an important first step in our analytical pipeline, allowing us to observe distinctive absorption features and reflectance patterns characteristic of each meat type. This preliminary examination helped establish baseline expectations about the separability of the classes and informed subsequent preprocessing strategies.

The reflectance spectra for each type of zhambon were averaged to facilitate clearer visualization and interpretation. Figure 6 presents the mean reflectance spectra obtained from three types of zhambon samples across the visible to near-infrared (VNIR) region. Distinct spectral patterns can be observed among the samples, reflecting differences in their biochemical composition and tissue structure. In the visible range (approximately 400–600 nm), beef zhambon exhibits markedly lower reflectance compared to turkey and chicken, consistent with its higher concentration of myoglobin and other pigment compounds that strongly absorb visible light. Turkey and chicken hams display similar spectral profiles in this region, though chicken shows slightly higher reflectance in the green to red bands (around 480–620 nm).

As the wavelength increases toward the red and near-infrared regions (600–900 nm), all samples show a general rise in reflectance, a characteristic response to reduced pigment absorption and increased light scattering within the tissue. Among the three, turkey maintains the highest reflectance, followed by chicken and beef. Subtle differences in the spectral slope and local peaks around 760–800 nm likely correspond to variations in water and fat content, as well as microstructural scattering differences between the meat types.

Overall, the Figure highlights clear separability between beef and the poultry samples, particularly in the visible range, where pigment absorption dominates. The relative similarity between turkey and chicken suggests that finer spectral features or derivative-based analyses may be necessary to achieve accurate discrimination between these two classes. These observations reinforce the suitability of spectral information for meat-type classification and justify the use of DL approaches capable of capturing subtle spectral correlations.

### 3.2. Binary Classification Results (chicken vs. beef)

The binary classification task focused specifically on differentiating between spectral signatures of beef and chicken zhambon samples. This emphasis on binary classification (beef versus chicken) was strategically chosen due to practical market considerations. According to industry reports, the most prevalent form of meat product fraud in consumer markets involves the substitution of less expensive chicken meat in products labeled as premium beef zhambon. This economic motivation stems from the significant price differential between beef and chicken products, creating financial incentives for fraudulent substitution practices. Both our 1D-CNN

and LSTM architectures demonstrated high performance in this binary classification scenario, achieving high accuracy in distinguishing between the spectral signatures of these two meat types.

The CNN architecture proved to be effective for this task. The training history illustrated in Figure 7 reveals a stable learning process, with both training and validation accuracy curves converging smoothly toward optimal performance. It should be noted that for illustrating the training process, we included the evaluation of just one experimental run out of five replications for visual clarity; however, across all five runs, the training progress exhibits similar convergence and stability. This convergence pattern indicates the model successfully extracted discriminative spectral features while avoiding substantial overfitting issues, which is particularly noteworthy given the relatively limited training dataset. The validation accuracy plateaued at 100%, confirming the model's robust capability to generalize from the training data to unseen samples. This high generalization capability is further substantiated by the comprehensive performance metrics on the independent test set presented in Table 1, which shows precision, recall, and F1-scores exceeding 99% for both beef and chicken classes, culminating in an impressive average F1-score of 99.87±0.17.

The LSTM network similarly exhibited notable classification capabilities, effectively capturing the sequential dependencies within the spectral signatures. This architecture's ability to model long-range dependencies in sequential data proved highly advantageous for analyzing the subtle progressive changes across the electromagnetic spectrum that characterize different meat proteins and lipid compositions. The training progression depicted in Figure 8 demonstrates efficient learning dynamics, with the model (in one of our experimental runs) ultimately achieving a validation accuracy of 100%, matching the CNN's performance.

The detailed performance metrics for the LSTM model on the test set (Table 1) reinforce these observations, yielding perfect precision, recall, and F1-scores of 99.94±0.17% across both classes. This high performance underscores the LSTM's aptitude for capturing the intricate spectral patterns that differentiate beef from chicken zhambon samples, even when these differences may be subtle to visual inspection.

While both architectures achieved comparable classification accuracy, minor differences emerged in their computational efficiency profiles. The CNN architecture required a longer absolute training time as reported in Table 1 which aligns with expectations given its multiple convolutional and pooling layers. However, an examination of the convergence patterns in Figure 7 and Figure 8 reveals that the CNN model actually reached optimal performance in fewer training iterations than the LSTM model.

This convergence efficiency advantage of the CNN architecture can be attributed to its spatial feature extraction capabilities, which effectively capitalize on the localized spectral features characteristic of meat samples. The convolutional layers efficiently detect distinctive absorption bands and reflection patterns within specific wavelength regions, allowing for faster feature learning. In contrast, while the LSTM architecture eventually achieved equivalent accuracy, it required additional training iterations to fully capture the sequential dependencies across the spectral range.

These computational efficiency considerations become particularly relevant in practical deployment scenarios where rapid model training or updating might be required to accommodate new reference samples or adapt to different hyperspectral sensor configurations. The faster convergence of the CNN model suggests it may offer advantages in scenarios requiring frequent model retraining, despite its longer absolute training time.

### 3.3 Multi-class Classification

The multi-class classification task presented a considerably more challenging problem than the binary classification, requiring our models to differentiate between beef, chicken, and turkey zhambon samples simultaneously. This increased complexity arises from the need to establish decision boundaries among three classes in the high-dimensional spectral feature space rather than a single boundary in the binary case. Despite this elevated complexity, both our CNN and LSTM architectures demonstrated notable adaptability and classification prowess.

The training progression visualized in Figure 9 and Figure 10 reveals that both models effectively learned discriminative features from the spectral data while successfully avoiding overfitting, which is particularly noteworthy given our relatively constrained dataset size. The CNN architecture exhibited a healthy and stable learning trajectory, ultimately achieving a validation accuracy of 93.40%. In comparison, the LSTM model demonstrated superior performance with a validation accuracy reaching 98.51%, indicating its enhanced capability to capture the sequential dependencies in spectral signatures that differentiate between the three meat types.

A detailed examination of the performance metrics presented in Table 2 provides quantitative evidence of each model's classification capabilities on an independent test set. The LSTM architecture consistently outperformed the CNN across all key metrics, including precision, recall, and F1-scores for all three classes. The LSTM model achieved an impressive average F1-score of 98.12%, compared to the CNN's still-commendable 93.89%. This performance differential suggests that the sequential modeling capacity of LSTM networks is particularly well-suited to capturing the subtle spectral variations that distinguish different meat products.

The confusion matrix depicted in Figure 11 further corroborates the LSTM model's robust classification ability. The predominance of predictions along the diagonal of the matrix indicates high classification accuracy across all classes, with minimal misclassifications. The limited confusion that does occur appears primarily between chicken and turkey classes, a finding that aligns with our spectral analysis reported in section 3.1.

The mean reflectance spectra for beef, chicken, and turkey samples provide critical insights into the underlying reasons for the observed classification performance, particularly regarding the challenges in discriminating between poultry products. As revealed in Figure 6, visual inspection of these spectral signatures demonstrates a significant overlap between chicken and turkey zhambon across the measured wavelength range (400-990 nm).

The poultry spectra exhibit remarkably similar reflectance patterns, with nearly identical absorption valleys and reflectance peaks. This pronounced spectral similarity can be attributed to the comparable biochemical composition of chicken and turkey meats—specifically their water, protein, and fat content distributions, which are the primary constituents influencing light absorption and reflection in this spectral range. The processing methods applied to transform these poultry meats into zhambon products (including curing, smoking, and other preservation techniques) have not introduced sufficient biochemical differentiation to create easily distinguishable spectral fingerprints within this specific wavelength range.

In stark contrast, beef zhambon displays a markedly distinct spectral signature characterized by different overall reflectance intensity and unique absorption features at specific wavelengths. This clear spectral differentiation explains the consistently high-performance metrics observed for the beef class across both classification models. The distinctive reflectance characteristics of beef can be attributed to its fundamentally different muscle fiber composition, myoglobin content, and fat distribution compared to poultry products.

These spectral observations provide a scientific foundation for interpreting the classification results and highlight the high capability of our models—particularly the LSTM architecture—to discern even subtle spectral differences between highly similar meat products. The models' ability to differentiate between chicken and turkey despite their spectral similarities demonstrates the power of advanced neural network architectures in extracting discriminative features that may not be immediately apparent through visual inspection of spectral curves.

### 3.4 Comparison to Traditional ML Algorithms

The performance of traditional ML algorithms is assessed in Table 2. SVM obtained an accuracy of 72.43% with moderate macro F1-score (70.99), indicating difficulties in capturing non-linear separability among chicken, turkey, and zhambon spectra. SVM struggled to effectively differentiate between the spectral signatures of the different meat types, suggesting that the complexity of the problem exceeds what can be captured by the kernel-based approach with our selected features.

RF performed well, reaching 94.44% accuracy and a macro F1-score of 94.40%, suggesting that ensemble methods effectively exploit feature variability. The strong performance indicates that the RF classifier successfully captured the discriminative patterns in the statistical features derived from hyperspectral data.

GB achieved the best traditional ML results, with 94.65% accuracy and a macro F1-score of 94.61%, highlighting its ability to model complex non-linear relationships between statistical features and meat classes. The superior performance of GB among traditional ML methods demonstrates its effectiveness in handling the intricate patterns present in meat authentication tasks.

While ensemble-based methods (RF and GB) performed competitively with DL approaches, there are notable differences:

- CNN and LSTM operate directly on the spectral sequences, eliminating the need for manual feature extraction. This allows them to learn discriminative spectral patterns end-to-end, whereas traditional ML relies on pre-defined statistical descriptors.
- LSTM outperformed all traditional ML classifiers with an average accuracy of 98.12%, marginally higher than gradient boosting. It is notable that the standard deviation of the LSTM accuracy (0.76%) is much less than others, which confirms its ability in providing consistent and reliable predictions across different experimental runs. Its advantage lies in modeling sequential dependencies across wavelengths, which handcrafted statistical features cannot fully capture. LSTMs are particularly effective at learning long-range dependencies in sequential data through their specialized memory cell architecture, which includes input, forget, and output gates that regulate information flow.
- In terms of computational efficiency, the classical ML models had low training time (in the order of tenths of a second), although the feature extraction also requires time. DL models required more training resources but omit the feature extraction time.

These results suggest that while ensemble-based ML methods (RF and GB) remain strong contenders for hyperspectral classification when using engineered statistical features, DL methods provide additional benefits by leveraging raw spectral sequences. LSTM, in particular, demonstrated its ability to slightly surpass gradient boosting, reflecting the importance of capturing sequential spectral dependencies in the wavelength domain. Moreover, CNN and LSTM avoid the manual effort and potential bias of feature engineering, offering a more generalizable and scalable solution for meat authentication.

The performance difference between traditional ML and DL methods highlights a fundamental tradeoff: traditional methods offer computational efficiency and interpretability but rely on the quality of hand-crafted features, while DL provides superior performance through automatic feature learning but at the cost of increased computational requirements and reduced interpretability. For applications where computational resources are limited or where feature engineering expertise is readily available, ensemble methods like GB present a viable alternative to DL approaches.

## 4. Conclusion

This study demonstrates the significant potential of hyperspectral imaging combined with DL models for non-destructive differentiation between chicken, turkey, and beef zhambon. Both 1D-CNN and LSTM models achieved high classification accuracy, with LSTM showing slightly superior performance at 98.12±0.76% compared to CNN's 94.61±1.97%. These results highlight the capacity of DL approaches to extract and leverage discriminative spectral patterns without requiring manual feature engineering.

While traditional ML methods like GB and RF performed admirably when provided with carefully crafted statistical features, DL models offered the advantage of end-to-end learning directly from raw spectral data. The LSTM's ability to model temporal dependencies across the wavelength dimension proved particularly valuable, allowing it to capture subtle spectral relationships that statistical descriptors might miss. This sequential modeling capability explains its marginal performance edge over both CNN and traditional approaches in challenging classification scenarios.

The comparative analysis between traditional and DL methods reveals important tradeoffs in computational efficiency versus performance. Traditional methods require less computation time for training but necessitate domain expertise for feature extraction. In contrast, DL models demand greater computational resources but eliminate the need for manual feature engineering, potentially offering more generalizable solutions for diverse food authentication challenges.

These findings pave the way for real-time food authentication systems in industrial and commercial settings, reducing the risk of food fraud and enhancing consumer trust. The high classification accuracy achieved in this study demonstrates that hyperspectral imaging, when coupled with appropriate ML techniques, can serve as a suitable tool for meat authentication in commercial supply chains. Such systems could be integrated into processing facilities for continuous quality control and authentication verification.

Our future work will focus on several key directions to enhance the practical applicability of this approach:

- Expanding the dataset to include more meat types, meat samples adulterated with different percentage levels of species substitution, various processing methods, and different storage conditions to improve model robustness across diverse real-world scenarios.
- Testing hybrid DL architectures, particularly CNN-LSTM combinations, to leverage the complementary strengths of both approaches—CNN's spatial feature extraction capabilities and LSTM's sequential modeling abilities.
- Investigating transfer learning techniques to enable rapid adaptation to new meat types with minimal additional training data.
- Developing more lightweight model architectures suitable for implementation in portable hyperspectral devices for real-time, on-site applications.

- Exploring model interpretability techniques to provide insights into the specific spectral regions most critical for authentication, potentially enhancing both performance and practical utility.

This research contributes to the growing body of evidence supporting the effectiveness of artificial intelligence in food science and safety applications. By continuing to refine these techniques, we move closer to creating accessible, reliable tools for ensuring food authenticity throughout the supply chain, ultimately protecting both consumers and legitimate producers from the consequences of food fraud.

### Acknowledgements

### Funding

### Declaration of Competing Interest

The authors declare no competing interests.

### Informed Patient Consent

This study used processed meat samples as experimental materials; no human participants or patient data were involved.

### References

[1] Sun, X., Wang, S., & Jia, W. (2024). Research progress of electronic nose and near-infrared spectroscopy in meat adulteration detection. Chemosensors, 12(3), Article 35. https://doi.org/10.3390/chemosensors12030035

[2] Yu, Y., & others. (2025). Meat species authentication using portable hyperspectral imaging. Frontiers in Nutrition, 12, Article 1577642. https://doi.org/10.3389/fnut.2025.1577642

[3] Arnalds, T., McElhinney, J., Fearn, T., & Downey, G. (2004). A hierarchical discriminant analysis for species identification in raw meat by visible and near infrared spectroscopy. Journal of Near Infrared Spectroscopy, 12(3), 183–188. https://doi.org/10.1255/jnirs.424

[4] Mortas, M., Awad, N., & Ayvaz, H. (2022). Adulteration detection technologies used for halal/kosher food products: An overview. Discover Food, 2(1), Article 15. https://doi.org/10.1007/s44187-022-00015-7

[5] Li, Y., Wang, H., Yang, Z., Wang, X., Wang, W., & Hui, T. (2024). Rapid non-destructive detection technology in the field of meat tenderness: A review. Foods, 13(10), Article 1512. https://doi.org/10.3390/foods13101512

[6] Wang, Y., Teo, E., Lin, K. J., Wu, Y., Chan, J. S. H., & Tan, L. K. (2023). Quantification of pork, chicken, beef, and sheep contents in meat products using duplex real-time PCR. Foods, 12(15), Article 2971. https://doi.org/10.3390/foods12152971

[7] Chaudhary, V., Kajla, P., Dewan, A., Pandiselvam, R., Socol, C. T., & Maerescu, C. M. (2022). Spectroscopic techniques for authentication of animal origin foods. Frontiers in Nutrition, 9, Article 979205. https://doi.org/10.3389/fnut.2022.979205

[8] Pirhadi, S., Shariatifar, N., & Pirhadi, M. (2024). Identification of animal species in meat products using chemometrics-based high-performance liquid chromatography: A systematic review. Journal of Biochemicals and Phytomedicine, 3(1), 53–58. https://doi.org/10.34172/jbp.2024.11

[9] Lu, B., Dao, P. D., Liu, J., He, Y., & Shang, J. (2020). Recent advances of hyperspectral imaging technology and applications in agriculture. Remote Sensing, 12(16), Article 2659. https://doi.org/10.3390/rs12162659

[10] Ma, J., Sun, D.-W., Pu, H., Cheng, J.-H., & Wei, Q. (2019). Recent developments of hyperspectral imaging systems and their applications in detecting quality attributes of red meats: A review. Annual Review of Food Science and Technology, 10, 119–140. https://doi.org/10.1146/annurev-food-032818

[11] Pu, H., Sun, D.-W., & others. (2023). Recent advances in muscle food safety evaluation: Hyperspectral imaging analyses and applications. Critical Reviews in Food Science and Nutrition, 63(22), 1–20. https://doi.org/10.1080/10408398.2022.2059377

[12] Kheiralipour, K., Sajadipour, F., & Nadimi, M. (2025). A review of nut quality assessment using hyperspectral imaging technique. Journal of Food Composition and Analysis, 108, Article 108184. https://doi.org/10.1016/j.jfca.2025.108184

[13] Kheiralipour, K., Sajadipour, F., & Nargesi, M. H. (2025). Applications of spectral imaging in biosystems engineering in Iran, a review. Recent Progress in Sciences, 2(1), Article 007. https://doi.org/10.70462/rps.2025.2.007

[14] Zhang, Y., Zheng, M., Zhu, R., & Ma, R. (2022). Adulteration discrimination and analysis of fresh and frozen-thawed minced adulterated mutton using hyperspectral images combined with recurrence plot and convolutional neural network. Meat Science, 192, Article 108900. https://doi.org/10.1016/j.meatsci.2022.108900

[15] Ince, V., Bader-El-Den, M., Esmeli, R., Maurya, L., & Sari, O. F. (2025). Predicting spoilage intensity level in sausage products using explainable machine learning and GAN-based data augmentation. Food and Bioprocess Technology. Advance online publication. https://doi.org/10.1007/s11947-025-03971-x

[16] Yu, Y., Chen, W., Zhang, H., Liu, R., & Li, C. (2024). Discrimination among fresh, frozen–stored and frozen–thawed beef cuts by hyperspectral imaging. Foods, 13(7), Article 973. https://doi.org/10.3390/foods13070973

[17] Siddique, A., & others. (2025). Development of predictive classification models and extraction of signature wavelengths for the identification of spoilage in chicken breast fillets during storage using near infrared spectroscopy. Food and Bioprocess Technology, 18(1), 933–941. https://doi.org/10.1007/s11947-024-03499-6

[18] Zheng, X., Li, Y., Wei, W., & Peng, Y. (2019). Detection of adulteration with duck meat in minced lamb meat by using visible near-infrared hyperspectral imaging. Meat Science, 149, 55–62. https://doi.org/10.1016/j.meatsci.2018.11.005

[19] Kamruzzaman, M., Sun, D.-W., ElMasry, G., & Allen, P. (2013). Fast detection and visualization of minced lamb meat adulteration using NIR hyperspectral imaging and multivariate image analysis. Talanta, 103, 130–136. https://doi.org/10.1016/j.talanta.2012.10.045

[20] Cruz-Tirado, J. P., & others. (2024). Detection of adulteration of alpaca (Vicugna pacos) meat using a portable NIR spectrometer and NIR-hyperspectral imaging. Journal of Food Composition and Analysis, 126, Article 105901. https://doi.org/10.1016/j.jfca.2023.105901

[21] Edwards, K., Hoffman, L. C., Manley, M., & Williams, P. J. (2023). Raw beef patty analysis using near-infrared hyperspectral imaging: Identification of four patty categories. Sensors, 23(2), Article 697. https://doi.org/10.3390/s23020697

[22] Bai, Z., & others. (2024). Establishment and comparison of in situ detection models for foodborne pathogen contamination on mutton based on SWIR-HSI. Frontiers in Nutrition, 11, Article 1325934. https://doi.org/10.3389/fnut.2024.1325934

[23] Jiang, H., Yang, Y., & Shi, M. (2021). Chemometrics in tandem with hyperspectral imaging for detecting authentication of raw and cooked mutton rolls. Foods, 10(9), Article 2127. https://doi.org/10.3390/foods10092127

[24] Sentandreu, M. Á., & Sentandreu, E. (2015). Authenticity of meat products: Tools against fraud. Food Research International, 77, 236–246. https://doi.org/10.1016/j.foodres.2014.03.030

[25] Al-Sarayreh, M., Reis, M. M., Yan, W. Q., & Klette, R. (2018). Detection of red-meat adulteration by deep spectral–spatial features in hyperspectral images. Journal of Imaging, 4(5), Article 63. https://doi.org/10.3390/jimaging4050063

[26] Zhu, H., Gowen, A., Feng, H., Yu, K., & Xu, J. L. (2020). Deep spectral-spatial features of near infrared hyperspectral images for pixel-wise classification of food products. Sensors, 20(18), 5322. https://doi.org/10.3390/s20185322

[27]   Xiong, Z., Sun, D. W., Zeng, X. A., & Xie, A. (2014). Recent developments of hyperspectral imaging systems and their applications in detecting quality attributes of red meats: A review. Journal of Food Engineering, 141, 1–13. https://doi.org/10.1016/j.jfoodeng.2014.02.004

[28]   Huang, H., Liu, L., & Ngadi, M. O. (2014). Recent developments in hyperspectral imaging for assessment of food quality and safety. Sensors, 14(4), 7248–7280. https://doi.org/10.3390/s140407248

[29]   Jia, W., van Ruth, S., Scollan, N., & Koidis, A. (2022). Hyperspectral imaging (HSI) for meat quality evaluation across the supply chain: Current and future trends. Current Research in Food Science, 5, 813–823. https://doi.org/10.1016/j.crfs.2022.05.016

[30]   Vercammen, A., & others. (2011). Shelf-life extension of cooked ham model product by high hydrostatic pressure and natural preservatives. Innovative Food Science & Emerging Technologies, 12(4), 407–415. https://doi.org/10.1016/j.ifset.2011.07.009

[31]   Parto Afzar Sanat. (2025). Desktop hyperspectral imaging system. https://www.partoafzar.ir/.

[32]   Liu, Y., Dang, B., Li, Y., Lin, H., & Ma, H. (2016). Applications of Savitzky-Golay filter for seismic random noise reduction. Acta Geophysica, 64(1), 101–124. https://doi.org/10.1515/acgeo-2015-0062

[33]   Choi, J. H., & others. (2022). Hyperspectral imaging-based multiple predicting models for functional component contents in Brassica juncea. Agriculture, 12(10), Article 1515. https://doi.org/10.3390/agriculture12101515

[34]   Shiddiq, M., Candra, F., Anand, B., & Rabin, M. F. (2024). Neural network with k-fold cross validation for oil palm fruit ripeness prediction. Telkomnika, 22(1), 164–174. https://doi.org/10.12928/TELKOMNIKA.v22i1.24845

[35]   Ruffin, C., King, R. L., & Younan, N. H. (2008). A combined derivative spectroscopy and Savitzky-Golay filtering method for the analysis of hyperspectral data. GIScience & Remote Sensing, 45(1), 1–15. https://doi.org/10.2747/1548-1603.45.1.1

[36]   Cortes, C., & Vapnik, V. (1995). Support-vector networks. Machine Learning, 20(3), 273–297. https://doi.org/10.1007/BF00994018

[37]   Breiman, L. (2001). Random forests. Machine Learning, 45(1), 5–32. https://doi.org/10.1023/A:1010933404324

[38]   Friedman, J. H. (2001). Greedy function approximation: A gradient boosting machine. The Annals of Statistics, 29(5), 1189–1232. https://doi.org/10.1214/aos/1013203451

[39]   Kingma, D. P., & Ba, J. (2015). Adam: A method for stochastic optimization. arXiv. https://doi.org/10.48550/arXiv.1412.6980

[40]   Goodfellow, I., Bengio, Y., & Courville, A. (2016). Deep learning. MIT Press.
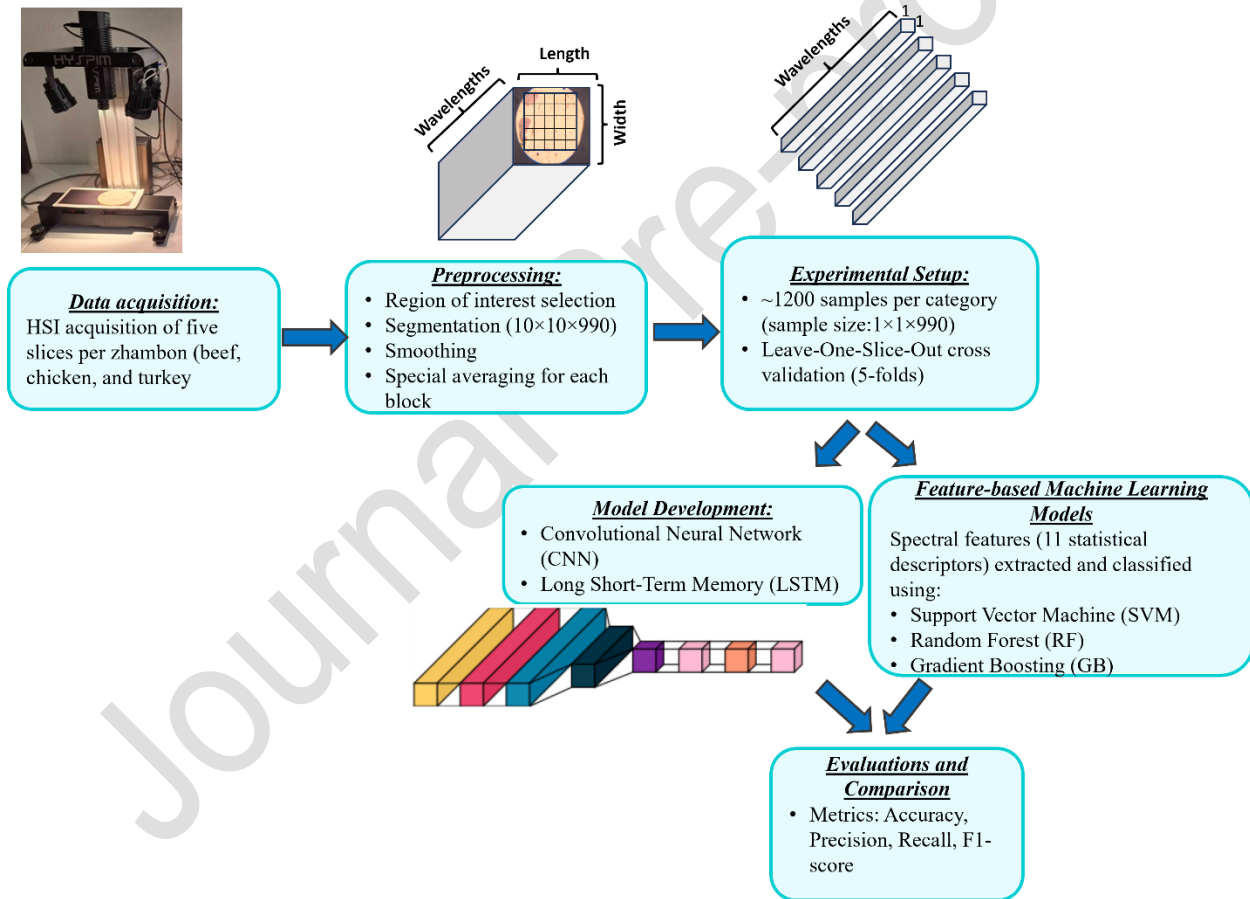
[41]



**Figure 1. Overview of the study workflow for zhambon type identification using hyperspectral imaging and machine learning approaches. Hyperspectral images of beef, chicken, and turkey zhambon samples were acquired, preprocessed, and analyzed using both deep learning-based models and traditional feature-based machine learning algorithms. Model performance**

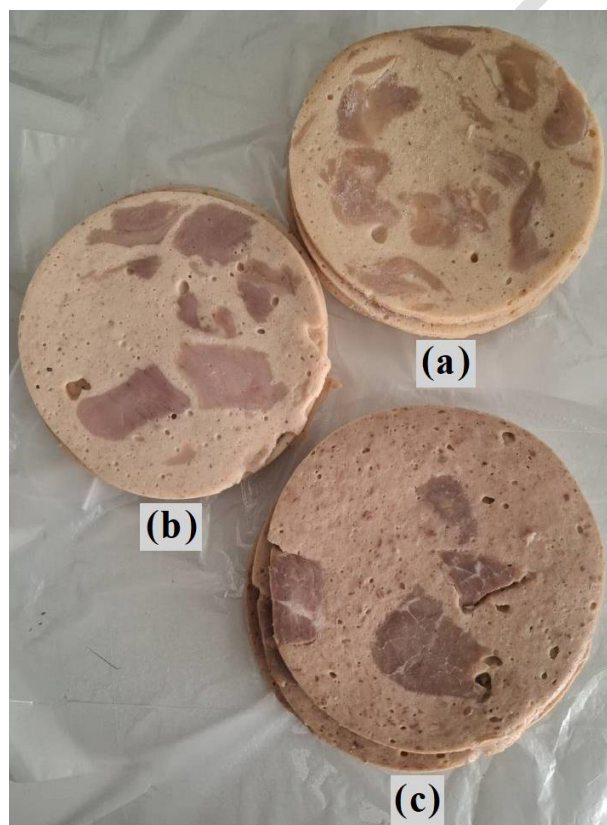was evaluated using multiple metrics to enable comprehensive comparison across all classification approaches

**Figure 2. Prepared samples of (a) chicken, (b) turkey, and (c) beef zhambons**
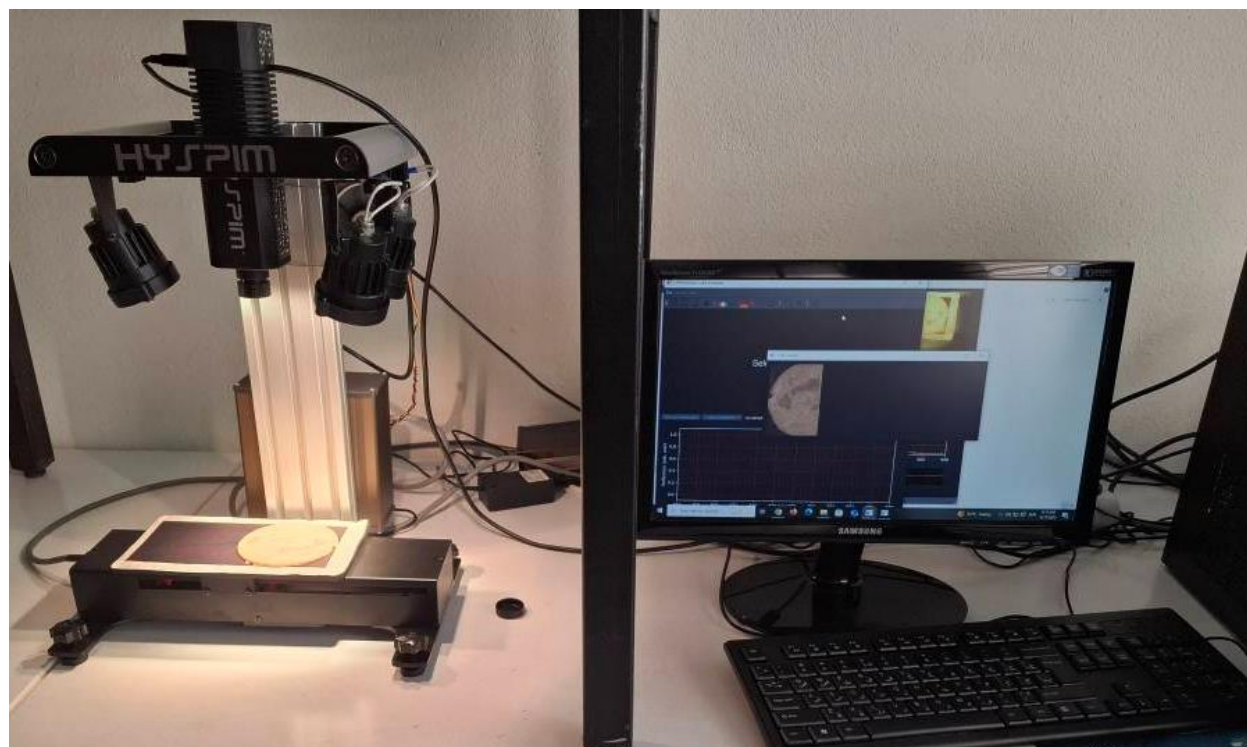
**Figure 3. Setup of hyperspectral imaging system**

**Figure 4. The designed one-dimensional convolutional neural network architecture**
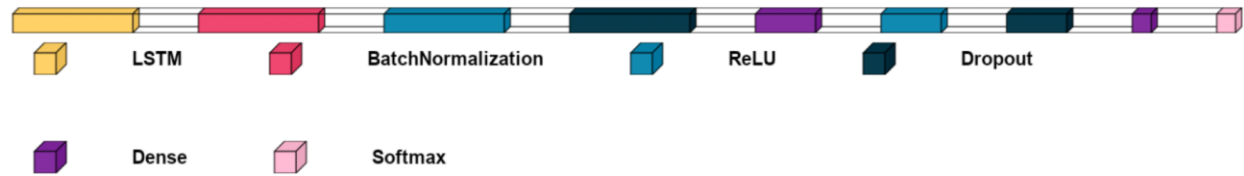
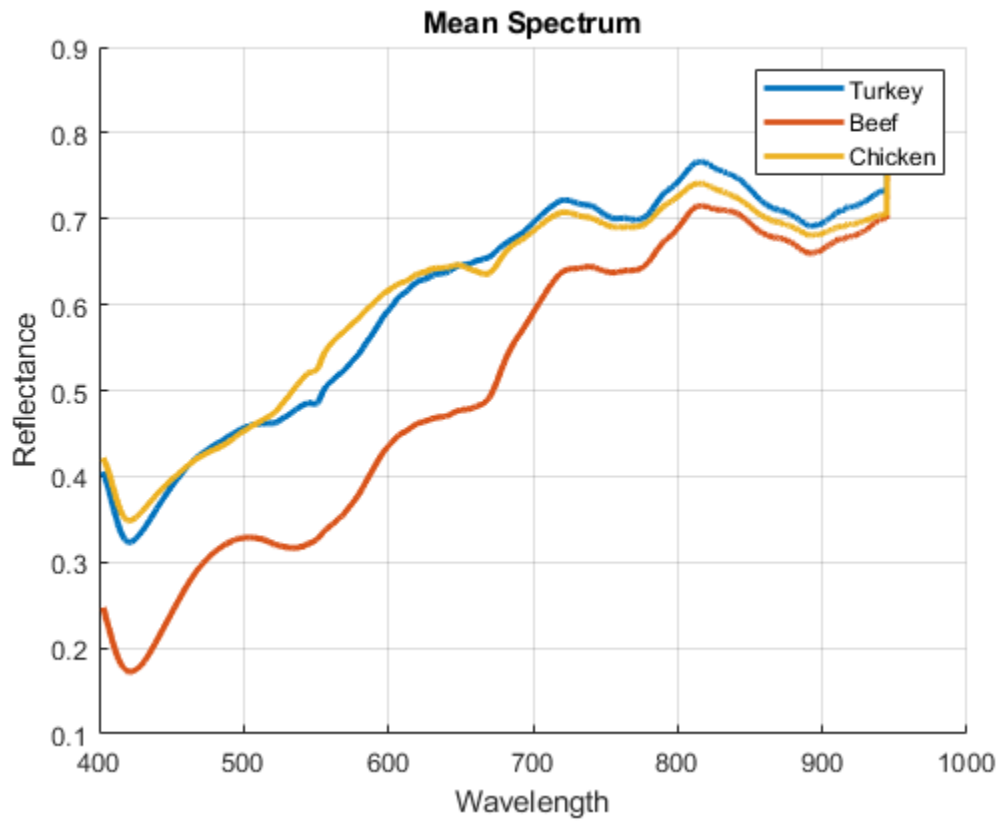**Figure 5. The designed long short-term memory architecture**

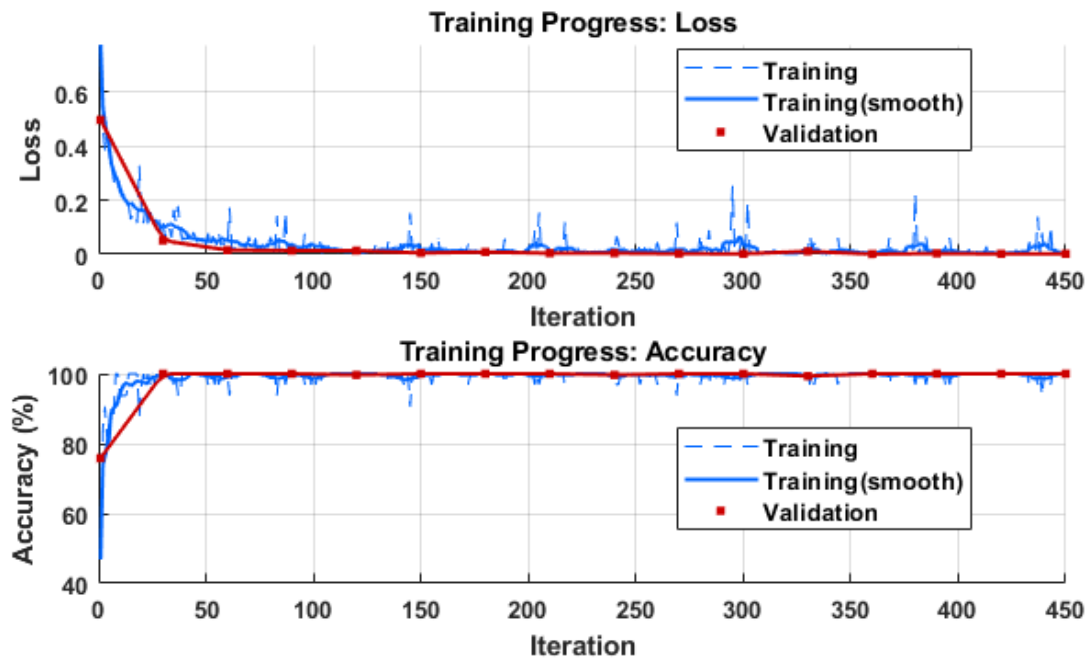**Figure 6. Mean reflectance spectrum for three types of zhambon**

**Figure 7. Training progress of the one-dimensional convolutional neural network model for binary classification between beef and chicken samples.**
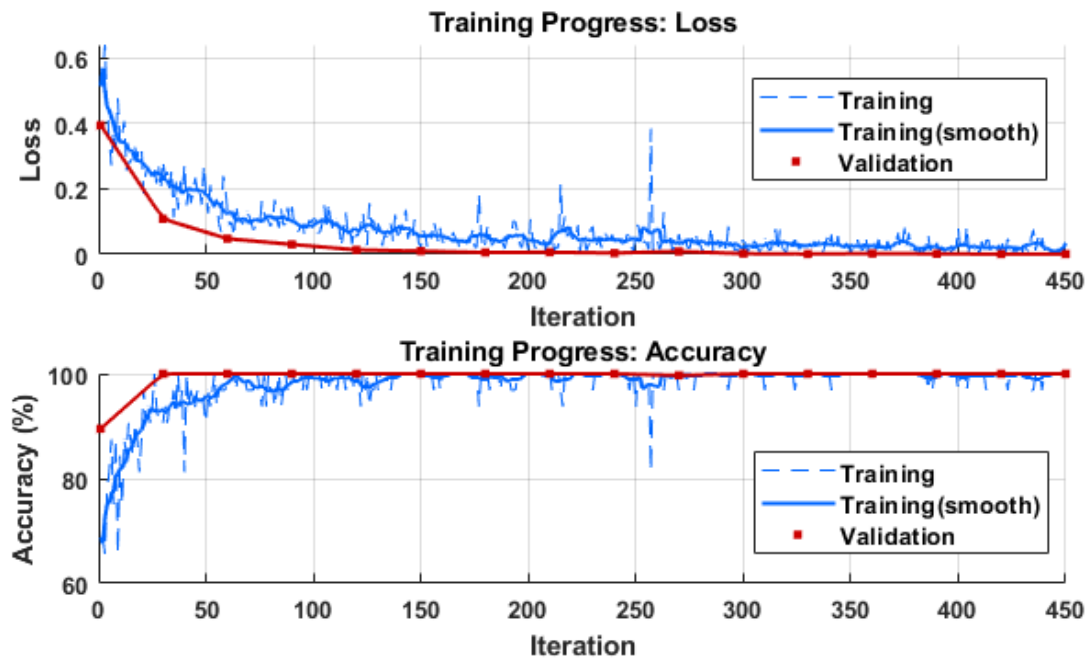
**Figure 8. Training progress of the long short-term memory model for binary classification between beef and chicken samples**

**Figure 9. Training progress of the one-dimensional convolutional neural network model for classification between beef and chicken, and turkey samples**
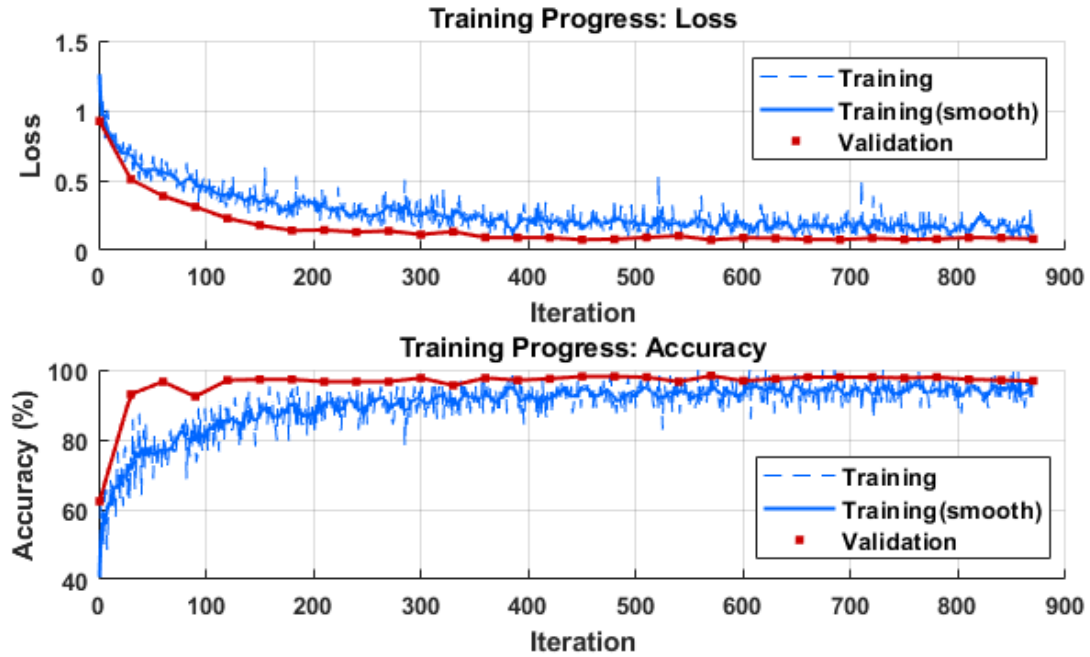
**Figure 10. Training progress of the long short-term memory model for classification between beef and chicken, and turkey samples**
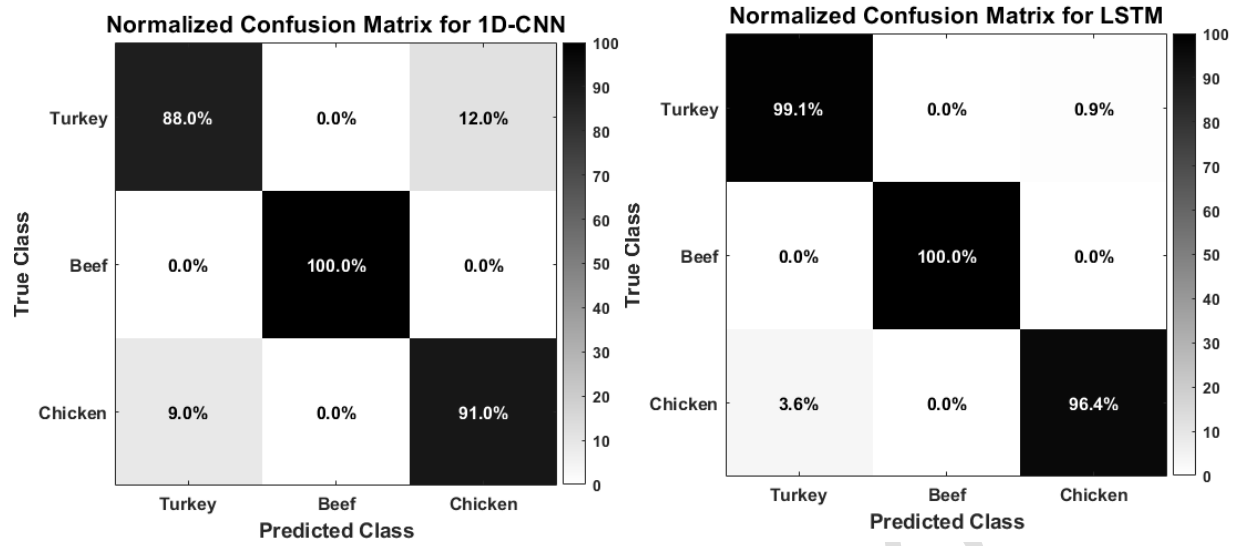
**Figure 11.** Confusion matrix of the one-dimensional convolutional neural network and long short-term memory models for classification between beef, chicken, turkey zhambon samples

**Table 1. Evaluation of the models for binary classification between beef and chicken samples.**

| Method | Accuracy (%) | Precision (%) | Recall (%) | F1-score (%) | Training time (seconds) |
|---|---|---|---|---|---|
| One-Dimensional Convolutional Neural Network | 99.87±0.17 | 99.87±0.17 | 99.87±0.17 | 99.87±0.17 | 21.85 |
| Long Short-Term Memory | 99.94±0.16 | 99.94±0.16 | 99.94±0.16 | 99.94±0.16 | 15.43 |

**Table 2. Performance evaluation of traditional machine learning models and deep models in multi-class classification of beef, chicken, and turkey zhambon samples.**

| Method | Accuracy (%) | Precision (%) | Recall (%) | F1-score (%) | Training time (seconds) |
|---|---|---|---|---|---|
| Support Vector Machine | 72.43±3.78 | 71.65±4.48 | 72.29±3.79 | 70.99±3.64 | 0.84 |
| Random Forest | 94.44±2.17 | 94.42±2.23 | 94.42±2.19 | 94.40±2.21 | 0.82 |
| Gradient Boosting | 94.65±1.76 | 94.63±1.81 | 94.63±1.77 | 94.61±1.80 | 0.97 |
| One-Dimensional Convolutional Neural Network | 94.61±1.97 | 94.00±1.04 | 93.90±1.06 | 93.89±1.05 | 75.47 |

| Long Short-Term Memory | 98.12±0.76 | 98.12±0.77 | 98.12±0.77 | 98.12±0.77 | 47.65 |
|---|---|---|---|---|---|

| Long Short-Term | 98.12±0.76 | 98.12±0.77 | 98.12±0.77 | 98.12±0.77 | 47.65 |